Theoretical and Experimental Analysis of a Non Contacting Elastohydrodynamic Sealing

Matthias Scherrer* and Rudolf Scheidl

Institute of Machine Design and Hydraulic Drives, Johannes Kepler University, Linz, Austria
E-mail: Matthias.Scherrer@jku.at; Rudolf.Scheidl@jku.at
**Corresponding Author*

Received 30 November 2021; Accepted 17 August 2022;
Publication 29 April 2023

Abstract

This paper presents a novel elastohydrodynamic sealing concept for the contactless sealing of spool valves. The basic goal is that the spool and the sleeve can be manufactured with standard mechanical engineering precision. High initial gaps are compensated for the elastic deformation of an elastomer seal driven by a self-regulating hydrodynamic effect. The final gap reveals a small leakage within the range normal for precisely manufactured spool valves and also features a low friction since a direct, solid contact between the seal and the sleeve is prevented. This sought-after behavior in ideal conditions is compared with imperfect situations by means of a simulation study and experiments. The simulation uses a Finite Element model which takes the seal's elastic deformation, the mechanical contact, the sealing gap pressure and the surface roughness into account. A simple prototype of the sealing system was produced to test its functionality in real conditions. Leakages of $Q_{Leak} \leq 18\frac{ml}{min}$ @180 bar were recorded. However, an unexpectedly

International Journal of Fluid Power, Vol. 24_2, 141–170.
doi: 10.13052/ijfp1439-9776.2421

high friction occurred indicating an actual contact between the seal and the sleeve. The component roughness was identified as the cause of this behavior.

Keywords: Elastohydrodynamics, non-touching seal, spool valve.

1 Introduction

Gap sealings are standard in valves and special cylinders to ensure a very low friction. Contacting seals – common in hydraulic cylinders – cause substantial friction. The friction force F_f depends on various conditions, such as the pressure, speed, viscosity and sealing material and type. A coarse estimate of the order of magnitude is $F_f \approx p\ d\ \pi$ 0.01 N/(mm.bar), which reflects, for instance, the measurements of [1]. For very small cylinder diameters in particular, e.g. such as those used in exoskeletons, the friction forces relative to the hydraulic forces increase due to the large circumference to area ratio. A high friction hinders free movement, which is favorable in certain phases of human locomotion, for instance during the swing phase when walking. In precise valves, the manufacturing of narrow sealing gaps is still a substantial quality issue which, in turn, is also a cost issue. The high costs of servo-valves compared to proportional valves are substantially related to their higher precision [2]. The diameter clearances of spool valves are in the range of 4 to 20 μm [3], depending on the spool diameter, valve overlap and valve type. The leakage increases with the third power of clearance and is inversely proportional to the gap length. Hence a low leakage and low overlap inevitably require high precision manufacturing, which conventional machine shops cannot accomplish. This is an issue in the experimental testing of new ideas in academic research, for instance, in the authors' research group's work on hydraulic exoskeleton drives. The problems of high leakage in the first prototype of a valve system for a digital cylinder drive for exoskeletons are reported in [4].

This difficulty gave birth to the idea to investigate elastohydrodynamic sealing concepts. The goal is to find a mechanism which compensates high initial gaps by elastic deformation to reduce the leakage to acceptable values. In addition, the mechanism has to avoid the direct contact of the seal with its counter-surface to avoid dry friction forces. The idea of using elastohydrodynamic effects in hydraulics is not new. In [5] the wear problems in valves of Diesel common rail injectors were found to be caused by an adverse

elastohydrodynamic effect which created a high contact force between the actuator piston and the bore. By making some small changes to the design, it was possible to resolve these problems by reversing this effect and avoiding contact by introducing a small design change. The pressure-induced elastic deformation of the properly designed slender sealing lands of a fast switching valve can have a similar centering effect for a valve spool to overcome valve sticking [6]. The simulations and experiments reported in [7] demonstrate that a sealing gap between the cylindrical rod and the multi-conical bore of a plastic sleeve produces a pressure field which stabilizes the rod at the centerline if there is either a difference in pressure between both gap ends or the rod performs an axial motion. The essential mechanism consists of the elastic deformation of the sleeve and the hydrodynamic coupling. Textured radial shaft seals use elastohydrodynamic effects to create an oil film if the shaft rotates when the seals touch the shaft during a standstill. A structure such as this can even pump back oil from the air to the oil side under pressure to make the leakage almost zero [8, 9]. A structured sealing surface is applied in face seals to avoid contact when the system is running. If the shaft speed is at a rated value, centrifugal forces can be used to compensate for a difference in pressure over the seal for zero leakage [10, 11]. In [12] a sealing concept is proposed for turbomachinery which employs self-adjusting, so called "hydrodynamic runners" to obtain very small but never-touching sealing gaps for a very small leakage. To this end, sealing pressure forces which tend to close the gap are counteracted by hydrodynamic forces in a self-adjusting manner. In terms of quality, this operating principle is closest to the concept presented in this paper. Other classical non- touching seals, like the standard gap seal, the labyrinth seal and the threaded shaft seal, rely on small gap heights with a high hydraulic valve manufacturing precision.

The basic idea of the sealing concept presented in this paper was first proposed and studied in an approximate axisymmetric, analytical model and corresponding numerical simulations in [13]. It differs from the established sealing concepts due to its ability to compensate for high initial gaps and the avoidance of contact. The present paper is more general in terms of geometric situations, imperfections and the role of surface roughness and it employs advanced mathematical models and experimental investigations. The sealing concept is presented in Section 2. The Finite Element model to simulate different imperfections is described in Section 3 and the experimental results in Section 4. The conclusions and outlook in terms of further research work are provided in the last section.

2 Sealing Concept

Figure 1 depicts the basic sealing principle. The initial gap between the seal and the sleeve is h_0. It is assumed that since this is higher than in conventional gap seals, it will cause an excessive leakage. The sealing principle should be able to substantially reduce h_0 as a result of the pressure-induced deformation of the ring. If the gap height $h(x)$ is constant, the pressure distribution in the gap is linear, falling from p_A to p_B. The pressure on the inner face of the ring is uniformly p_A because the seal contacts the shoulder on the left side while there is a gap to the right shoulder and a gap exists on the inner side. The inner and outer pressure fields create a radial force which widens the ring and decreases the sealing gap. This widening is not uniform, since the inner to outer pressure difference $\Delta p(x)$ decreases from the B side to the A side. The B side will be widened more, leading to a smaller gap there. The resulting gap pressure field $p(x)$ has a small or even negligible gradient on the A side and a large gradient on the B side. This trend is more pronounced the smaller the gap on the B side becomes and approximates a constant pressure field, i.e. $p(x) \approx p_A$. In other words, $\Delta p(x)$ (see Figure 1) and its resultant radial

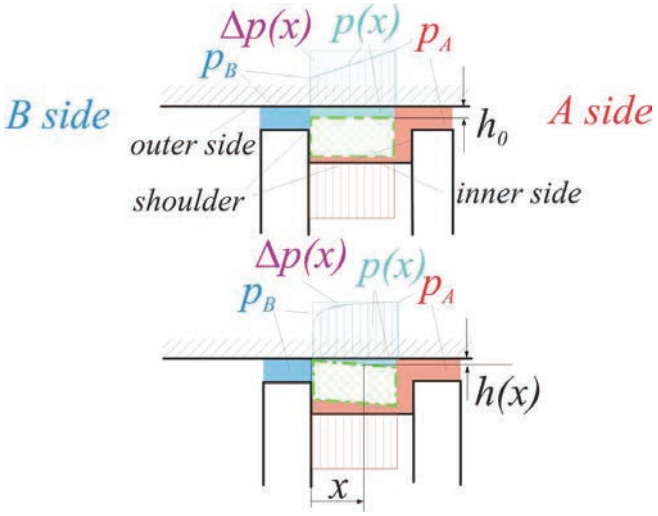

Figure 1 Operational principle of the hydrodynamic sealing concept: upper picture: seal in the initial position with a uniform gap h_0 and a corresponding linear gap pressure $p(x)$; lower picture: a deformed sealing ring with a variable gap height $h(x)$, gap pressure $p(x)$ and an inner to outer pressure difference $\Delta p(x)$.

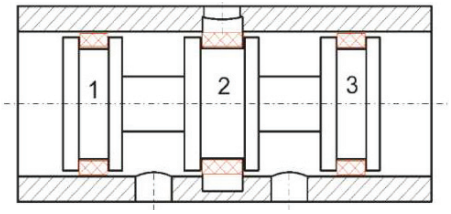

Figure 2 Planned application of the seal for a spool valve; sealing lands 1 and 3 are analysed; the sealing configuration of position 2 was not analysed.

force decrease the larger the deformation becomes and would become zero if the seal were to contact the counter face on the B side. Thus, no contact can occur and a certain gap always remains. In its current balanced state, the elastic deformation of the seal and the pressures on both sides are equal.

For symmetry reasons, the principle works equally for a reverse difference in pressure difference ($p_A < p_B$). Then the ring is pressed on the A side shoulder and the distribution of $h(x)$ and $p(x)$ are just the mirror images of the case ($p_A > p_B$).

Figure 2 depicts the principal arrangement of the seals in a valve spool. The seals are mounted loosely in circumferential grooves. The studied sealing concept is intended for the lands of the valve (# 1 and # 3 in Figure 2) where the counter face is uninterrupted. The sealing of land # 2, which forms the metering edges of a spool valve, requires different approaches and is, therefore, not addressed in this paper.

Pure PEEK (polyetheretherketone) is considered for the sealing ring. It is the toughest plastic material in terms of strength and stiffness (modulus of elasticity $=$ 4200 MPa, tensile strength $=$ 120 MPa, [14]) which is required for the manufacturing of prototypes using conventional machining processes. Furthermore, compared to other high tensile strength plastic materials like PAI, PEI, PPS or Nylon, PEEK has a very low friction when paired with steel components, which is advantageous for this application too, if mixed lubrication occurs [15].

This qualitative model of the working principle is based on the assumption of perfect geometries of the sleeve and sealing ring in terms of the shape and surface (no surface roughness), the pure elastic deformation of the ring, i.e. no plastic strains or creep. Furthermore, the relative motion of the seal to the counter face is neglected, which has an influence on $p(x)$ and $h(x)$ and in particular on the stability of the mechanism.

3 Simulation Model

3.1 Purpose and Basic Approach

The qualitative considerations on the working mechanism cannot explain the quantitative effects and the influence of the main design parameters thereon. Purely an experimental investigation is challenging, since a measurement of the gap height field, which is one of the main system states, is not feasible with the sensors available. Therefore, a detailed analysis is carried out using a numerical model of the sealing concept. This should reveal the detailed nature of the deformation mechanism and its coupling with the gap pressure field. The main outcomes are the gap height distribution, the pressure distribution and the leakage flow. One further purpose is the analysis of the influences of several imperfections related to manufacturing tolerances. Unfortunately, the simulation model is not able to explore the role of the surface roughness in sufficient detail and this is a game changer when it comes to mixed lubrication with partial, solid body contact. According to [16] the roughness increases, particularly static friction, if the sealing ring has contact with the counter face. This effect is modelled in a simplified way by a contact condition between both bodies. It becomes active where $h(x)$ falls below a value representing an equivalent surface roughness (h_{min} in Figure 3) of the seal and bore. With the minimum gap h_{min} the existing flow passages are modelled in a simplified manner due to asperities which allow leakages even in such contact situations.

It does not account for the anisotropy of the surface roughness, the possibility of closing local or global flow passages and the influence of the contact pressure on the flow passage situation of the asperities. Such effects are studied in [17–19]. The sealing concept is modelled as a coupled solid-fluid Finite Element problem, employing the Finite Element software ABAQUS.

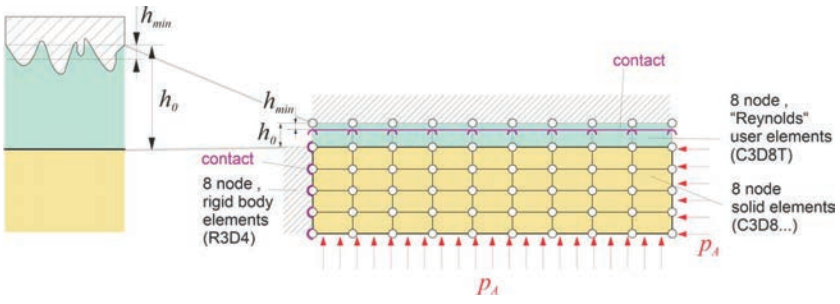

Figure 3 Longitudinal section and modeling features of the Finite Element model in ABAQUS.

Table 1 The extremum values of the Reynolds and Froude number calculated for two cases: small pressures with big gap heights and a big leakage; high pressures with small gap heights and a big leakage

Name	Parameter	Value
Leakage, simulated	$Q_{min...max}$	0.001…0.01 l/min
Gap heights used for simulation	$h_{gap,min...max}$	0.1…100 μm
Cross section, calculated	$A_{min...max}$	7.85e-9…7.82e-06 m^2
Velocities, calculated	$v_{min...max}$	0.021…21.2 m/s
Reynold's numbers, calculated	$Re_{1,2}$	$\langle$0.0524, 0.0521$\rangle$
Froude numbers, calculated	$Fr_{1,2}$	$\langle$0.096, 95.8$\rangle$
Ratios Re/Fr, calculated	$Re_{1,2}/Fr_{1,2}$	$\langle$0.54, 5.4e-4$\rangle$

Only the main components like the seal, the fluid gap and the interacting wall are taken into consideration. The fluid film is modelled using what is known as the Reynold's user element, which results in a much faster operation than the built-in procedure for solving the Navier Stokes equations [20]. This user element, programmed in FORTRAN, allows the finite element discretization of the Reynold's equation [7, 13] which is extended to cover sealing problems [21]. The Reynold's equation is an approximation of the Navier Stokes equation. It neglects inertial and gravitational terms [22] for flows in small gaps. These simplifications are justified by a small Reynold's number (Equation (1)) and a small relation of the Reynold's and Froude number (Equation (2)). Both numbers are provided in Table 1 for the parameters of Table 2.

$$Re = \frac{inertial}{friction} = \frac{\rho v L}{\eta} \ll 1 \tag{1}$$

$$Fr = \frac{inertial}{gravitational} = \frac{v^2}{gL};\ \frac{Re}{Fr} = \frac{gravitational}{friction} < 1 \tag{2}$$

The Reynolds elements are coupled by a so-called tie contact to the adjoining standard ABAQUS solid element which represents the seal (see Figure 3). The nodal forces of the slave nodes (gap) are estimated from the Reynold's user element pressure and influence the deformation of the seal elements.

The design parameters, the exemplary values applied in this paper, and the used element types can be found in Tables 2 and 3. The used element types are:

- C3D8 (8-node linear brick)

Table 2 The model parameters and exemplary values used in this paper. The friction coefficients chosen for the PEEK/steel pairing can be found in [23, 24]

Name	Parameter	Value
Length of the seal	L	5 mm
Outer diameter of the seal	D	25 mm
Height of the seal	h	0.5 mm
Initial gap height	h_0	$\langle 12, 32 \rangle$ μm
Modeled angle	φ	180°
Contact condition	h_{min}	$\langle 0, 4 \rangle$ μm
Dynamic viscosity	η	0.035 Ns/m^2
Density	ρ	0.86 kg/dm^3
Dry Friction (Neat PEEK/steel)	μ_{dry}	0.25
Wet Friction (Neat PEEK/steel, oil 30cSt, small time duration)	μ_{wet}	0.06

Table 3 Details of the finite element realization

Component	Element Number	Element Type	Material	Part
Seal	$20 \times 20 \times 4$	C3D8	PEEK	3D Deformable body
Gap	$20 \times 20 \times 1$	C3D8T	Fluid	3D Deformable body
Wall	44	R3D4	Steel	3D Discrete Rigid

- C3D8T (8-node thermally coupled brick, trilinear displacement and temperature, for the temperature potential, the hydraulic pressure is used instead)
- R3D4 (4-node 3D bilinear rigid quadrilateral)

Contacts occur on the seal's left head side and on its outer side if the sealing gap tends to become smaller than h_{min} (see Figure 3). This contact condition was also applied with the trivial value $h_{min} = 0$ μm in the cases without surface roughness modelling in order to avoid negative gap values. This could also occur in the case of the numerical iterations in ABAQUS and would violate the model validity. In ABAQUS a tie connection has to be defined between the Reynold's element layer and the outermost solid element layer of the sealing ring. The mechanical contacts are realized by the ABAQUS "Mechanical Contact" – condition, also taking into consideration the friction in the tangential direction, between the respective surfaces. The system pressure acts as a load and is ramped up linearly during the calculation run from $p_A = 0..250$ bar. To save computation time, the seal was modelled for only half of the circumference (180°) with adequate symmetry, boundary conditions.

3.2 Results of the Simulation with an Ideal Geometry and No Roughness

Figure 4 shows the displacement in the radial direction (the cylindrical coordinate system was used, U1 is the radial direction) for an ideal geometry (a perfectly cylindrical, homogenous sealing ring centrically placed in a perfect cylindrical sleeve and an overall constant initial gap height $h_0 = 12$ μm) of the sealing ring for the final step with the maximum applied pressure of $p_A = 250$ bar.

Figure 5 shows the seal deformation for different pressures. When a very small gap is reached on the low pressure side for high pressures, a further pressure increase of p_A does not reduce but rather widens the gap on the high pressure side (this can be seen bottom right in Figure 5). Figure 6 shows the computed leakage flow over p_A and the gap pressure distribution for a maximum p_A. The leakage (left picture) rises strongly for a very low p_A, because those pressures cause only a negligible deformation, the gap height is approximately h_0. But for pressures above $p_A = 5$ bar, the leakage decreases reaching a minimum at about $p_A = 40$ bar to then rise again. Up to this pressure, the deformation occurs mostly on the low pressure side leading to a very small gap there. When the pressure is increased further, the gap on the high pressure side increases which, in combination with the higher pressure, results in a bigger leakage. The gap pressure is constant in the circumferential direction for an ideal geometry. The highest pressure gradient can be found at the smallest gap, i.e. on the low pressure side. Figure 7 shows the evolution of the gap heights on both ends over p_A. In the unloaded state, the gap height is uniform. As the pressure increases, the height on the lower

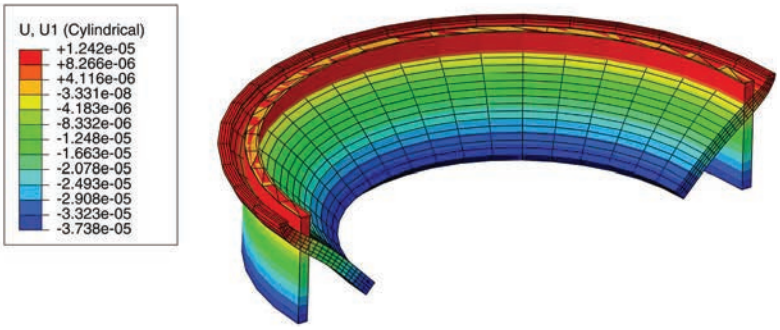

Figure 4 Initial and deformed shape of the seal in the radial direction of the seal given a boundary pressure of $p_A = 250$ bar, $p_B = 1$ bar and a displacement scale factor of 100; the deformation unit is in meters.

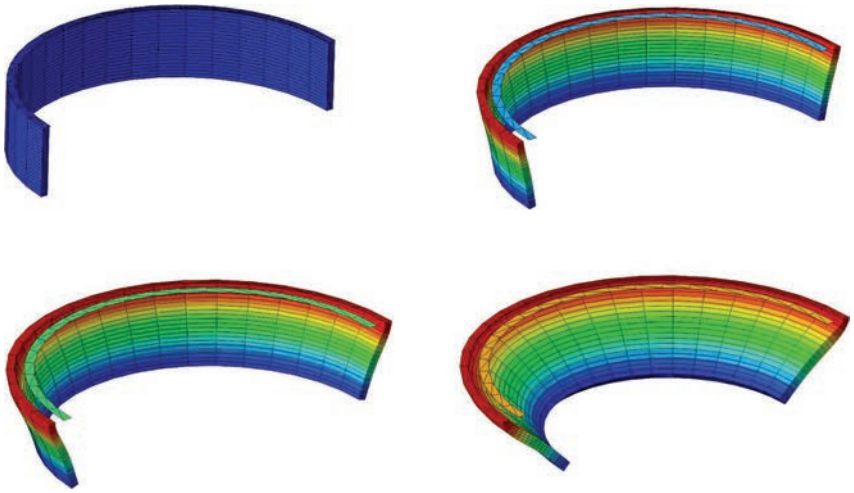

Figure 5 The seal in a deformed state for pressures $p_A = 0, 5, 60, 250$ bar (upper left, upper right, lower left, lower right), $p_B = 1$ bar; displacement scale factor: 100.

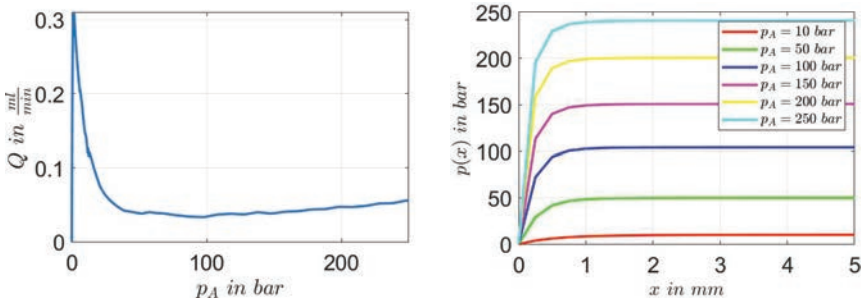

Figure 6 Simulation results; left: Leakage as a function of p_A; right: Axial gap pressure distribution over the length for different pressures p_A and $p_B = 1$ bar.

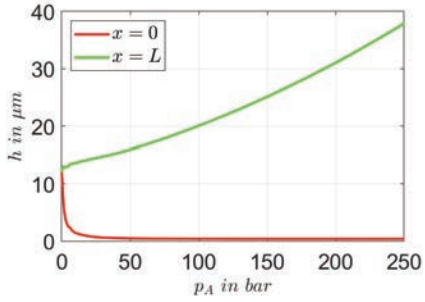

Figure 7 Simulated gap height at both seal ends over p_A.

pressure side ($x = 0$) decreases and drops down to a very small value of approx. $h = 0.5$ μm. The sealing gap on the high pressure side ($x = L$), as already discussed above, widens with a higher p_A.

3.3 Imperfection Analysis

The experiments reported in Section 4 revealed an unexpectedly high friction. To find the cause of this and, in turn, identify measures to overcome this problem, the role of several imperfections on the behaviour of the sealing system are analysed in this section. Imperfections of the initial gap geometry and the surface roughness were investigated. Of course, more types of deviations from the ideal model of the last section are possible and could influence the performance. Some examples are the non-uniformity of the sealing ring cross-section dimensions or of the material properties or residual-stresses which interfere with the stresses as a result of the deformation. The following selection of imperfections is an attempt to find one or more candidates able to explain the experimentally observed deviation from the behaviour expected. The investigated imperfections are:

- Eccentrically placed sealing ring
- Uneven circumferential gap
- Conical gap
- Rough surface

3.3.1 Eccentrically placed sealing ring

The cylindrical sealing ring can be moved radially in the spool notch, hence it may initially be placed eccentrically in the cylindrical sleeve. The initial situation is shown in Figure 8. The ring's radial displacements should compensate

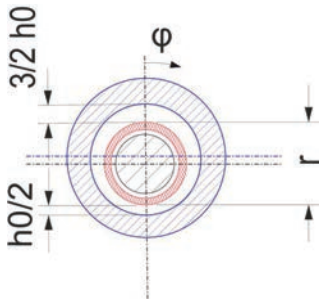

Figure 8 Eccentrical seal and piston in the sleeve; black: piston; red: seal; blue: sleeve.

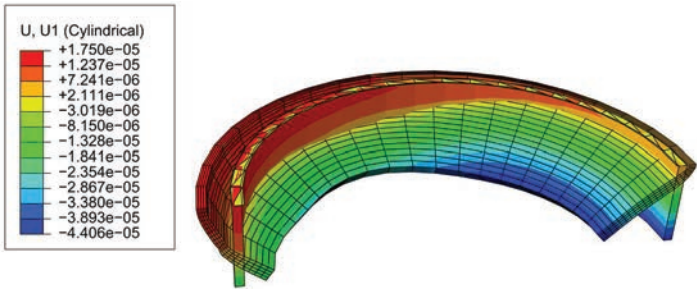

Figure 9 The initial and deformed shape of the seal in the radial direction of the initially, eccentrically placed seal for pressures $p_A = 250$ bar, $p_B = 1$ bar and a displacement magnification factor of 100.

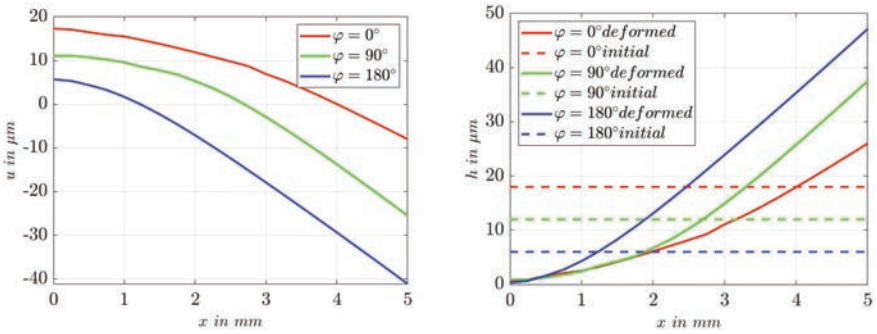

Figure 10 Sealing ring radial displacements and the resulting gap heights for the final pressure over the length of the seal.

for the eccentric placement. This may be hindered by the friction forces on the B side due to the frontal contact of the ring and the spool. This simulation case should clarify whether the sealing principle is strong enough to overcome this friction force.

The resulting deformation for $p_A = 250$ bar can be seen in Figures 9–11. Despite the initial non-uniformity, the final gap is uniform in the circumferential direction, approx. $h = 0.5$ μm on the low pressure side. Correspondingly, the ring displacement is non-uniform. For the circumferential position $\varphi = 180°$ where the initial gap is $\frac{h_0}{2}$, the displacement is much less than for $\varphi = 0°$, where it is $\frac{3h_0}{2}$. The deformation behaviour in the axial direction is qualitatively the same as for the perfect case. A small gap is reached even for moderate pressures on the low pressure side, while the ring moves away from the sleeve for higher pressures on the high pressure side.

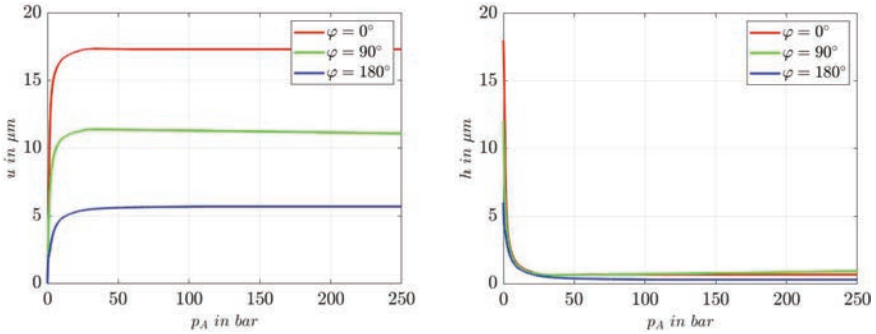

Figure 11 Radial displacement and the gap height for different pressures at three different angles in the circumferential direction on the low pressure side (point $x = 0$ mm).

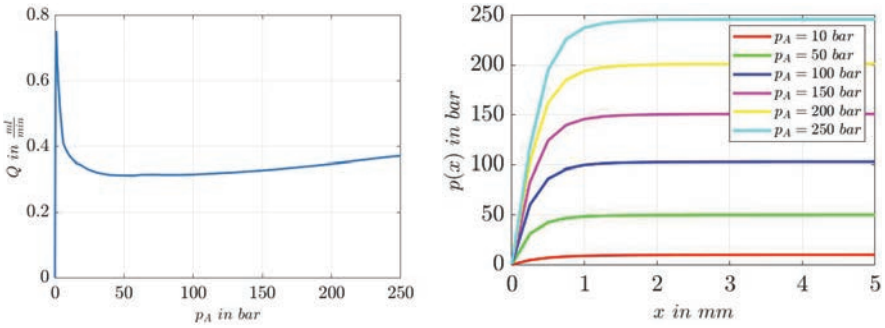

Figure 12 Leakage over system pressure and pressure distribution for different pressures p_A in the gap at the point $\varphi = 0°$.

The leakage given in Figure 12 differs only slightly from the ideal sealing depicted in Figure 6. In conclusion, the sealing ring eccentricity does not impair the functionality and cannot explain the high friction observed in the experiments.

3.3.2 Uneven circumferential gap

An uneven initial gap in the circumferential direction in the form of a cosine function $h(\varphi) = h_0(1+\frac{1}{2}cos(4\varphi))$ is set with the same value for $h_0 = 12$ μm as for the perfect case (Table 2), so $h(\varphi = 0°) = 18$ μm, $h(\varphi = 45°) = 6$ μm, $h(\varphi = 90°) = 18$ μm. The initial seal size remains the same. The resulting deformation of the seal can be seen in Figure 13. As expected, the seal's deformation compensates for the uneven initial gap and the final sealing gap is rather uniform. In Figure 14 the final displacements and heights of the

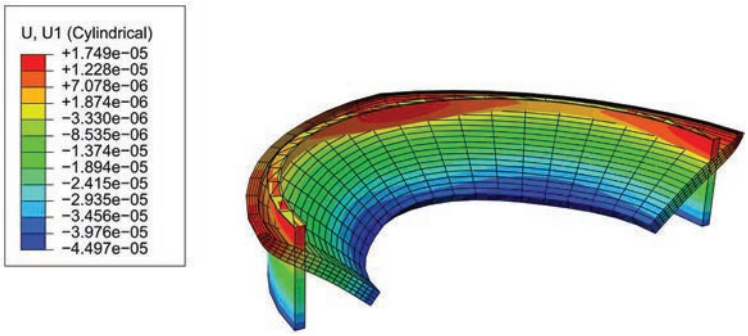

Figure 13 Initial and deformed shape of the seal in the radial direction with an uneven initial gap in the circumferential direction; boundary pressures: $p_A = 250$ bar, $p_B = 1$ bar; displacement magnification factor of 100.

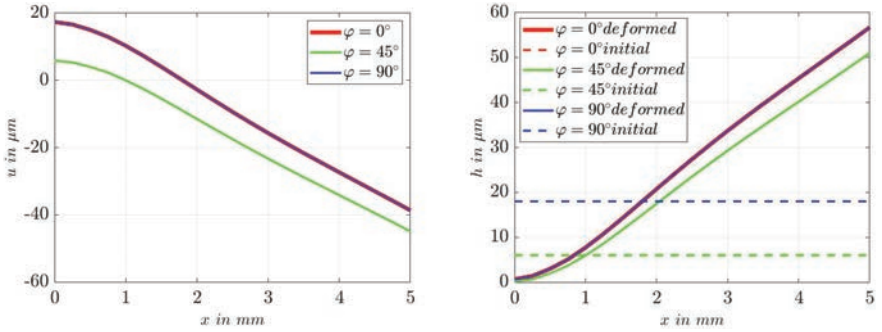

Figure 14 Sealing ring radial displacements (on the left) and the resulting gap heights for the final pressure over the length of the seal (on the right).

gap over the axial gap length are illustrated. The deformation of the seal in the angular position $\varphi = 45°$ is smaller than at $\varphi = 0°$ and $\varphi = 90°$ as the initial gap height is smaller. Figure 15 shows how the displacement and the height react for different input pressures p_A. Thus, the sealing principle works equally for this imperfection but the final leakage (compare Figure 16 with Figure 6) is approx. Four times higher than for the ideal settings.

3.3.3 Material roughness

In view of the very small final gap on the low pressure side in the micron or sub-micron range, the surface roughness of the seal and sleeve cannot be disregarded and have to be considered in a realistic model. The contact surface distance h_{min} of the model was approximated by the half sum of

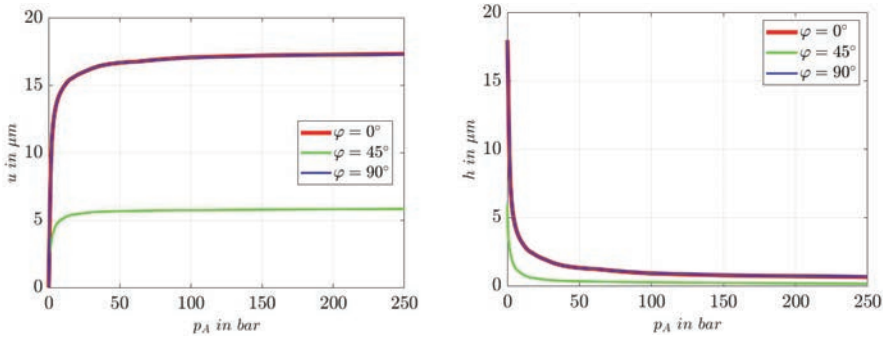

Figure 15 Radial displacement (on the left) and the height of the gap for different pressures (on the right) at three different angles in the circumferential direction on the significantly low pressure side (point $x = 0$ mm).

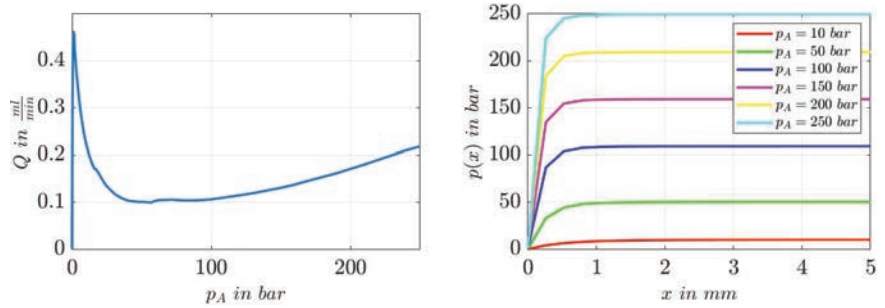

Figure 16 Leakage and pressure distribution of the gap at point $\varphi = 0°$.

the measured surface roughness (average R_z value of three measurements, see also Section 4) of the seal and sleeve as $h_{min} \sim \frac{R_{z,seal}+R_{z,sleeve}}{2} \sim \frac{5.4\mu\text{m}+2.6\mu\text{m}}{2} \sim 4\ \mu$m. This is a simple approach which delivered a reasonable explanation of the experimental results for leakage and friction given in Section 4. A more subtle consideration of the roughness, for instance according to [25], requires statistical roughness values which could not be obtained using the measurement device available. This was even more the case since an orthotropic roughness must be expected due to the manufacturing processes.

The seal model differs from the previous ones in two respects: (i) To lower the computation effort, a factually axisymmetric model is used. The ring is represented by a single row of elements stretching over an angle of $\varphi = 2.5°$, representing a sectorial cut with axisymmetric preserving boundary conditions on the cutting faces. This approach is used because the Reynolds

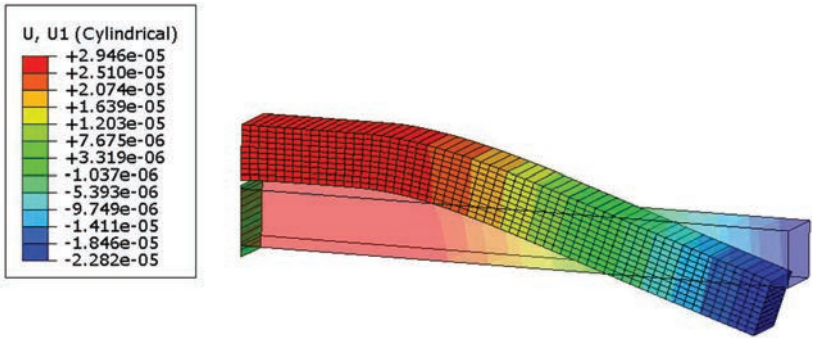

Figure 17 Initial and deformed shape of the seal in the radial direction computed by an axisymmetric model with a displacement magnification factor of 20 considering the roughness from a mechanical contact at $h_{min} = 4$ μm for $p_A = 250$ bar.

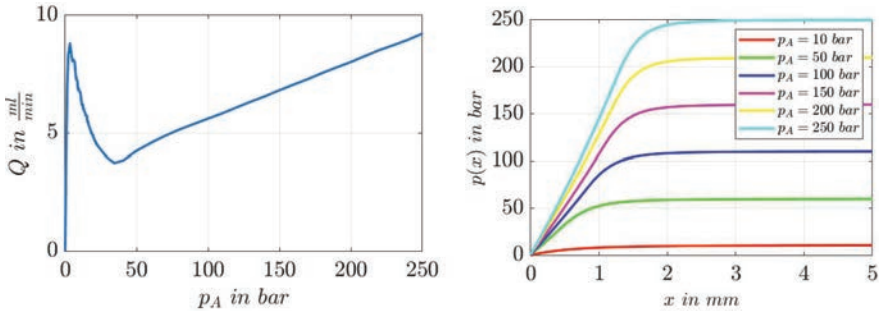

Figure 18 Leakage and pressure distribution in the gap for different pressures p_A.

element is only specified for two-dimensional gaps. (ii) A study was performed for an initial gap height of $h_0 = 32$ μm to confirm the experimental data reported in Section 4.

Figure 17 shows the computed deformed shape. What is virtually an asperity contact takes place on the low pressure side and the sealing ring is slightly compressed there. The surface roughness, modelled with a contact surface, leads to a much higher leakage than for smooth surfaces, which can be seen in Figure 18. Furthermore, the pressure distribution over the axial gap changes for higher values of p_A, as the gap is partly parallel on the low pressure side. The detailed radial displacement of the seal can be seen in Figure 19. The modelled surface roughness zone is shown in transparent light blue. Contact between the seal and the sleeve is noticeable for pressures higher $p_A = 50$ bar. Higher pressures extend the contact area which impacts the friction force behaviour as is noticeable in Figure 19. The coulomb

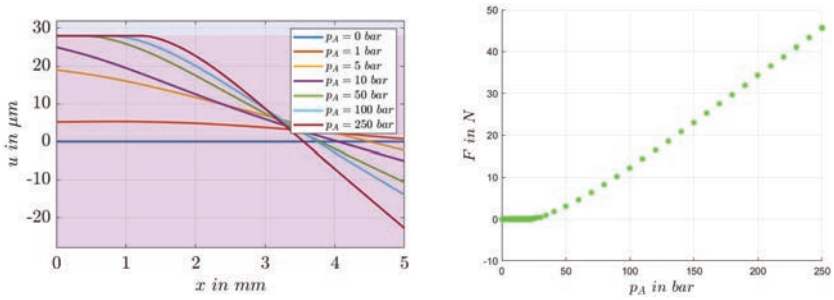

Figure 19 Radial displacements u over the length of the seal and the friction force F for different pressures p_A.

friction is calculated from the contact pressure of the elements multiplied with the responding friction coefficient. Friction occurs due to contact only and starts at $p_A \sim 40$ bar, rising approximately in a linear manner with the pressure. This rise stems from the increasing contact surface and the contact pressure.

3.3.4 Conical initial gap

The analysis of the effect of a conical initial gap on the sealing behaviour is carried out in combination with the roughness model introduced above, due to its significance [26]. An initial gap which diverges in the leakage direction (A $\rightarrow$ B) ($h_0(x = 0) = 20$ μm, $h_0(x = L) = 10$ μm) and a converging gap ($h_0(x = 0) = 10$ μm, $h_0(x = L) = 20$ μm) are simulated. The initial and deformed states for both cases are sketched in Figure 20. The piston and sleeve contours are marked by hatched areas. The red line indicates the contour of the surface asperities where a contact condition is formulated. The sloped initial gap is modelled by a correspondingly inclined sleeve contour. The displacement scale factor of 20 is also applied to the sleeve contour in order to show the gap evolution in a consistent manner. For a converging gap, the pressure in the gap is close to p_B in a wide range, since the small gap on the A side absorbs most of the pressure drop $p_A - p_B$. Thus, the seal is nearly loaded by a constant pressure difference $\Delta p(x) \approx p_A - p_B$ and deforms like a cylindrical shell with a constant inner pressure. This deformation pattern is disturbed by the contact forces where the seal has contact with the surface asperities' contact line (Figure 20a–d).

The behaviour of an initially converging gap is depicted in Figure 20e–h. The seal has contact with the sleeve on the smaller gap side first. For higher pressures p_A the seal – sleeve contact stretches across the full length.

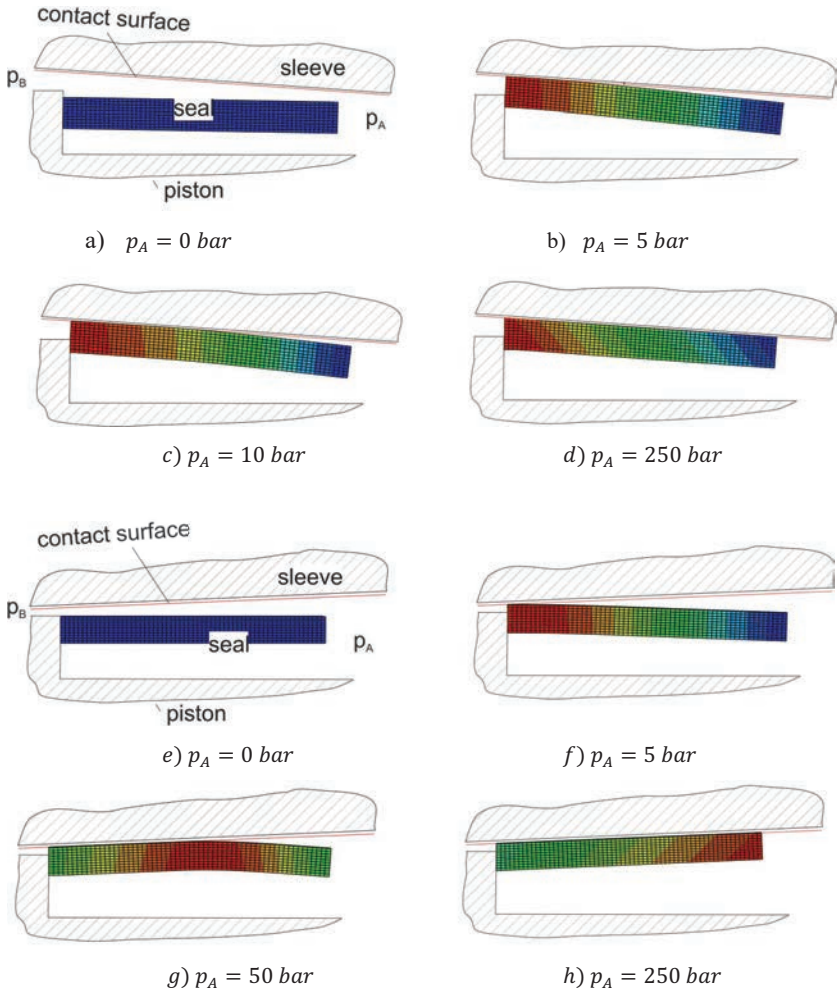

Figure 20 Deformed states of the seal for a diverging (cases a–d) and a converging (cases e–h) gap with piston, sleeve and contact line (red) contours. The scale factor for deformation is 20.

The converging gap cannot sufficiently counteract the detrimental role of the surface roughness. The resulting leakages, friction forces, displacements, and pressure drops can be seen in Figure 21. The higher friction forces result from the, on average, smaller initial gap which causes the first contact to already take place for small pressures.

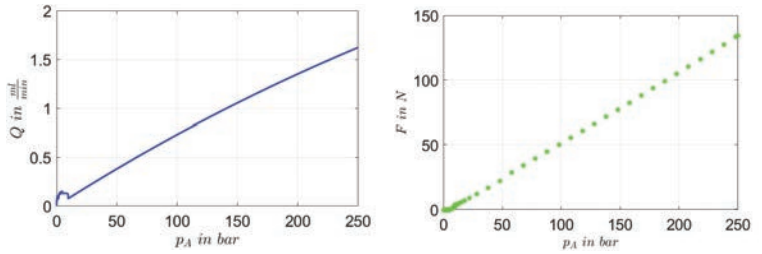

a) Leakage b) Friction force

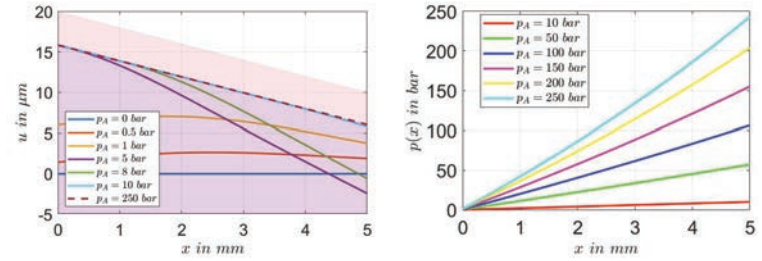

c) Radial displacements *d*) Pressure distributions

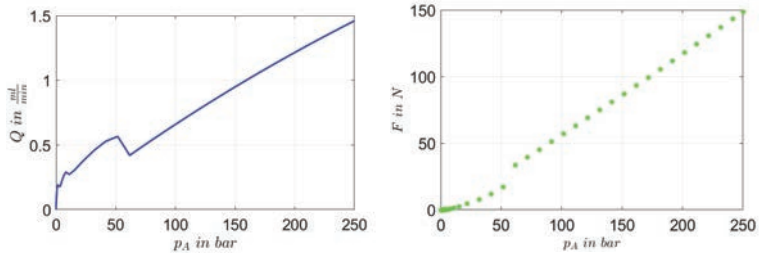

e) Leakage *f*) Friction force

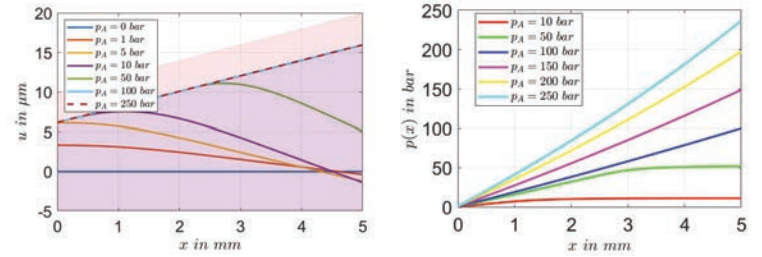

g) Radial displacements *h*) Pressure distributions

Figure 21 Leakage, friction force, radial displacement and pressure distribution for different pressure levels p_A; diverging gap: a–d; converging gap: e–h.

The imperfection analyses confirm the basic working principle but reveal the strongly deteriorating role of the surface roughness. However, moderate imperfections related to the main geometric dimensions of the sealing ring or the sleeve do not lead to a malfunctioning.

4 Test Rig and Experimental Results

A simple test rig was designed to experimentally analyse the sealing concept. Figure 22 portrays the piston with the seals in assembled and disassembled states. It consists of the spool, two sealing rings made out of PEEK, two groove rings and two screw nuts. The final parameters of the prototype can be found in Table 5. The test rig is demountable for an easy change of the seals. All of the components were manufactured in-house on a standard CNC turning machine. Manufacturing the seal with this machine is challenging due to the higher softness of PEEK compared to steel. It proved successful to create the drill hole of the seal first, and to mount the seal on a mandrel with the same diameter. Next, the outer diameter was turned and the ring was cut off. It is important to note that the front faces of the sealing ring were carefully ground to guarantee a smooth surface after the turning; without this step, the seal did not function at all. Furthermore, the bore of the sleeve was honed to achieve a smooth surface and reduce the effects of the surface roughness. The surface roughness in the axial direction of the seal and the sleeve were then measured with a perthometer as shown in Table 4. From those values h_{min} was calculated as described in 3.3.3. Figure 23 shows a schematic of the test rig and the assembled system with the measuring equipment. The two seals, the washers and the screw nuts are mounted on the piston before it is placed in the sleeve and covers are attached on both sides. To eliminate friction between the cover bore and the spool rods, the piston is continuously rotated and axially shifted while fixing the screws of the cover. A contactless magnetic position sensor on the left side facilitates measuring the motion and a piezoelectric force sensor allows the friction force to be measured

Figure 22 Piston with the seals and groove rings in an assembled (left) and disassembled (right) state (piston, seals, washers, screw nuts).

Table 4 Measuring equipment

Name	Principle	Type	Brand
Electromechanical cylinder	Spindle drive	LH 15	ROSE + KRIEGER
Force sensor	Piezoelectric	933 1B	Kistler
Displacement sensor	Magnetoresistive	MSS-975R, HA-705LK	Sony
Perthometer	Profile method	M1	Mahr

Table 5 Parameters employed for the prototype

Name	Parameter	Value
Length of the seal	L	5 mm
Outer diameter of the seal	D	25 mm
Height of the seal	h	0.5 mm
Measured initial gap height	h_0	28 & 32 μm
Contact condition	h_{min}	4 μm

(see Table 4 for details). It is placed between the electric linear drive and the piston. Fixating the system on the frame was done while permanently, slightly moving the electric cylinder to avoid restraint forces. This step is necessary after every mounting of the components, to obtain a smooth operation of the system. The recording of sensor signals (displacement, force) and the motion control of the piston via proper commands to the electric cylinder (pulse width modulation) were accomplished using MATLAB/Simulink and dSPACE. A simple PID controller, augmented with a velocity feed forward term was used for position control and tested for the different displacement points of the cylinder. A sine curve (amplitude $s = 12$ mm and frequency $f = 2\frac{\mathrm{rad}}{\mathrm{s}}$) was selected as the desired position trajectory. For the measurements, the pressure was adjusted in steps and the oil leakage was measured with a measuring cup for a time of 10 minutes, separately for every step. The leakage and force measurements were performed three times for each pressure level to check reproducibility.

To analyse the plain friction and the leakage, the first measurements were taken without any seal in the system. Figure 24 shows the leakage on the left side and the resulting friction force on the right side. A theoretical gap flow $Q_{theoretical} = \frac{bh^3}{12\eta l}\Delta p$ is provided for reference purposes. This is computed for the nominal gaps between the spool lands and the bore, which are 50 μm. Manufacturing inaccuracies are responsible for the difference between the left and the right leakage. The measured axial force for different pressures p_A shows some friction, most likely resulting from spool tilting [26]. This

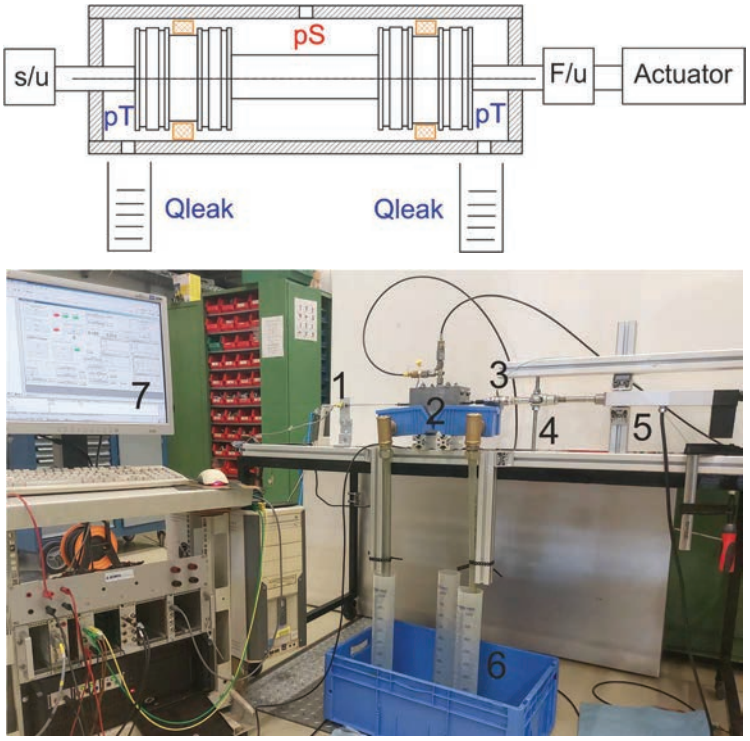

Figure 23 Test Rig: Schematic and photo of the experimental setup (1. Position sensor, 2. Assembled piston block, 3. Force sensor, 4. Guidance, 5. Electric cylinder, 6. Leakage measuring cup, 7. dSPACE control system).

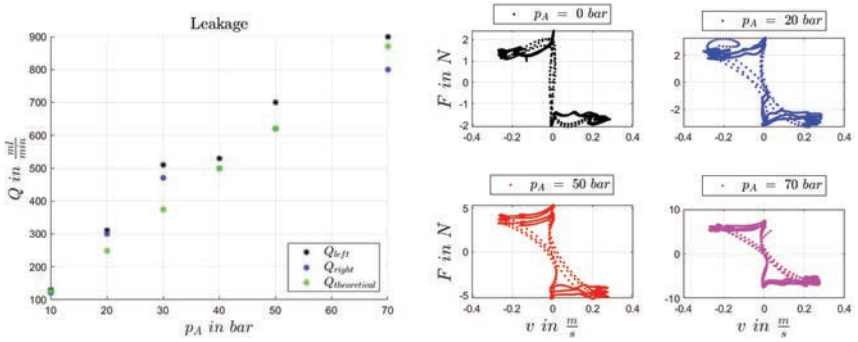

Figure 24 Leakage and friction force of the system without any seal for different pressures p_A.

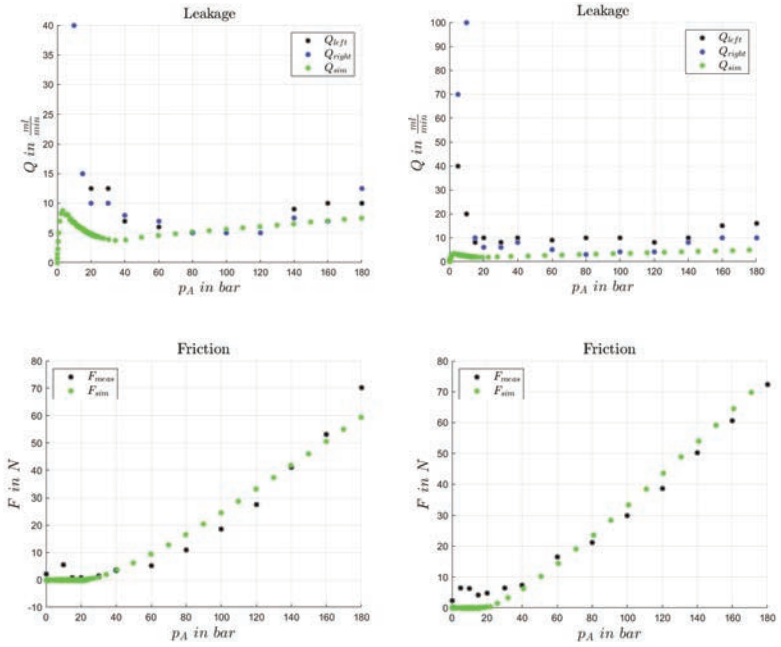

Figure 25 Measured and simulated leakage and total friction force for different pressures p_A and two different initial gap heights; left: $h_0 = 32$ μm; right: $h_0 = 28$ μm.

friction rises for higher pressures as the effect of tilting is stronger. These experiments only went up to $p_A = 70$ bar to keep the leakage measurement in a feasible range. Next, tests were performed with seals, as described above. The measured leakage and friction forces can be seen in Figure 25. Two different types of seals were used with slightly different outer diameters. The corresponding initial gap heights were $h_0 = 32$ μm and $h_0 = 28$ μm. For higher pressures ($p_A > 20$ bar) the measured leakage agrees well with the expected and simulated values, but not for lower pressures ($p_A < 20$ bar). A leakage between the seal and the piston as result of small gaps on the front face is assumed to be the reason, either due to surface roughness or due to the imperfect planarity of the seal front face. These gaps are likely closed for higher pressures p_A. The simulated friction was calculated from the contact pressure of the simulation model and a typical value for wet friction of $\mu_{wet} = 0.06$ (neat PEEK/steel with an oil lubricant of 30cSt, coefficient of friction taken from [23, 24]).

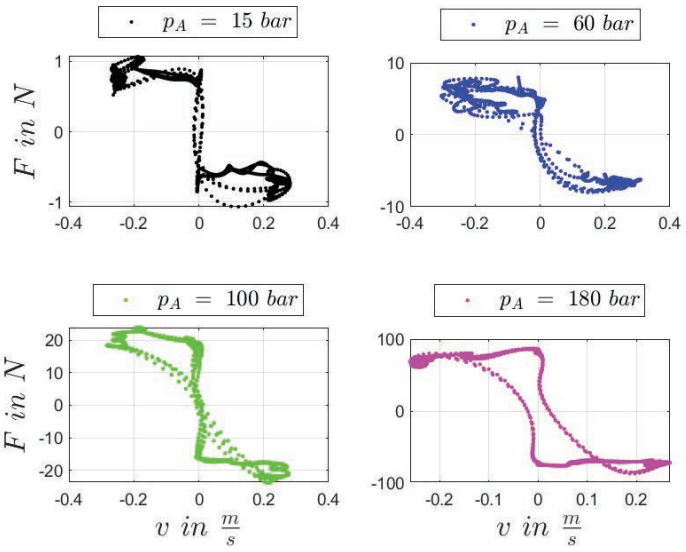

Figure 26 Measured friction force for different pressures p_A for an initial gap height $h_0 = 32\ \mu$m.

The friction forces in Figure 25 are the mean values of the absolute friction forces measured as shown in Figure 26. The measured friction forces presented here are the sum of both seals; a single seal would create only half of the value shown. For smaller pressures ($p_A < 20$ bar) the real friction forces measured are higher than for the simulated one. This is suspected to be the result of the spool tilting of the piston which also creates friction between the piston body and the sleeve. It should be noted that for the smaller initial gap height of $h_0 = 28\ \mu$m, the friction forces are slightly higher in the mid pressure range, but almost equal for the final pressure.

In conclusion, the measurements confirm the simulation results and the basic working principle of the sealing concept. These simple seals reduce the leakage of a standard gap seal system to approx. $\frac{1}{100}$ with the same initial gap height. Figure 26 shows that the working principle of the seal is not highly affected by a moving piston, provided pressure p_A exceeds a minimum value of approx. 20 bar. The achievable performances concerning the leakage (as shown in 3.2, which would ideally be more than 10 times lower) and the friction force (ideally zero) are mainly limited by the surface roughness. In the test rig, the roughness of the seal dominated, reflecting the difficulty to attain a high surface quality of the polymers using standard mechanical machining

processes. Injection moulding could deliver a much better surface quality bringing the sealing system into attractive performance ranges concerning both the leakage and friction. For cost reasons, manufacturing of this kind is generally serial production.

One weak point of the sealing concept is the unfavourable gap distribution in the length direction, with a small gap on the low pressure side where most of the full sealing pressure is absorbed. A different seal geometry with a more even pressure distribution would with a high probability produce better sealing results. A second deficiency is the high leakage at low pressures, as a result of the frontal side leakage and high initial radial gaps.

5 Summary and Conclusion

In touching hydraulic sealing concepts the setting leakage and friction are played off one against the other. The new concept presents a non-touching, hence a low friction sealing, with an acceptable leakage and with moderate manufacturing tolerances. The analysis of the concept in this paper confirms that the principle basically works and is robust w.r.t. several geometric imperfections but requires an extremely low surface roughness of the seal and sleeve to actually avoid contact and dry friction. The practicability of such surfaces in industrial manufacturing conditions, i.e. the injection moulding of the seal and the honing of the sleeve bore, cannot be confirmed without prototypes being produced. The intended elastic deformation does not have a favourable form since it leads to a very small gap on the low pressure side but gaps larger than the initial values on the high pressure side. This form results from the bending effect of the cylindrical shell in combination with the distribution of the gap pressure. The low gap which results in a very small leakage is likely to fall below the surface roughness leading to the high friction. Thus a sealing concept with a more even final gap distribution would be a better solution. The authors started to analyse sealing concepts featuring a different geometry, with which it was possible to adjust a minimum gap, which did not exhibit shell bending effects.

Acknowledgments

This work was sponsored by the COMET K2 Symbiotic Mechatronics and is funded by the Austrian Federal Government, the Federal State Upper Austria, and its Scientific Partners.

References

[1] X. Li, S. Suo, F. Guo, C. Wu, and X. Jia, (2018). A study of reciprocating seals with a new mixed-lubrication model based on inverse lubrication theory. Lubrication Science, 30(3), 126–136.

[2] A. Plummer Electrohydraulic servovalves – past, present, and future. Proc. 10th International Fluid Power Conference (10. IFK) March 8–10, 2016, Vol. 2, pp.

[3] Q. P. Chen, H. Ji, H. H. Xing, and H. K. Zhao, (2021). Experimental study on thermal deformation and clamping force characteristics of hydraulic spool valve. Engineering Failure Analysis, 129, 105698.

[4] M. Scherrer, R. Scheidl, S. Mittlböck (2019) Embodymentdesign of a hydraulic binary counter for exoskeleton use- problems and new solutions. In Proceedings of the 10th Workshop on Digital Fluid Power, February 28–March 1, 2019, Linz, Austria.

[5] R. Mitter: Rechnerische Untersuchung eines Verschleißproblems im Injektor eines Common Rail Dieseleinspritzsystems auf Basis eines elasto-hydrodynamischen Modells – Ventilkolbenführung und Dichtfunktion gegen Hochdruck. Diploma thesis, Johannes Kepler University Linz, Asutria, 2000.

[6] B. Winkler, G. Mikota, R. Scheidl, B. Manhartsgruber: Modelling and Simulation of the Elastohydrodynamic Behavior of Sealing Gaps, in Australian Journal of Mechanical Engineering (formerly Transaction of Mechanical Engineering), vol. 2, no. 1, 2005.

[7] C. Gradl and R. Scheidl. A Combined Hydrostatic Hydrodynamic Bearing Based on Elastic Deformation. Proceedings of the Proceedings of the 9th FPNI Ph. D. Symposium on Fluid Power : October 26–28, 2016, Florianoìpolis, SC, Brazil. 2016.

[8] W. Skolaut. Maschinenbau. Springer Vieweg. Springer-Verlag Berlin Heidelberg 2014.

[9] M. Schulz, M. Baumann, F. Bauer and W. Haas. Influence of different shaft surface finishes on the tribological and functional behaviour of radial shaft seals. Proceedings: 19th – 21th March 2018: 11th International Fluid Power Conference.

[10] M. Adjemout, N. Brunetiere and J. Bouyer. Numerical analysis of the texture effect on the hydrodynamic performance of a mechanical seal. 2016 IOP Publishing LtdSurface Topography: Metrology and Properties, Volume 4, Number 1.

[11] Y. Wang, J. Wang, H. Yang, N. Jiang, and X. Sun, (2004). Theoretical analyses and design guidelines of oil-film-lubricated mechanical face seals with spiral grooves. Tribology Transactions, 47(4), 537–542.

[12] E. Pedraza-Valle, G. Papageorgiou, A. Bowsher, P. F. Crudgington, C. M. Sangan, P. S. Keogh, and J. A. Scobie, (2019, June). On the Development of a Pressure Actuated Leaf Seal for Turbomachinery Applications. In Turbo Expo: Power for Land, Sea, and Air (Vol. 58653, p. V05BT15A009). American Society of Mechanical Engineers.

[13] C. Gradl. Hydraulic stepper drive : conceptual study, design and experiments. PhD thesis, Johannes Kepler University Linz, 2017.

[14] https://www.directplastics.co.uk/pdf/datasheets/PEEK%20Data%20Sheet.pdf, [Accessed: 09-March-2022].

[15] https://plasticranger.com/top-5-high-tensile-strength-plastics/, [Accessed: 09-March-2022].

[16] I. Krupka, P. Sperka, and M. Hartl, (2016). Effect of surface roughness on lubricant film breakdown and transition from EHL to mixed lubrication. Tribology International, 100, 116–125.

[17] D. Shen, and R. F. Salant, (2007). An unsteady mixed soft EHL model, with application to a rotary lip seal. *Tribology International*, *40*(4), 646–651.

[18] M. Scaraggi, G. Carbone, and D. Dini, (2011). Experimental evidence of micro-EHL lubrication in rough soft contacts. Tribology Letters, 43(2), 169–174.

[19] M. Scaraggi, J. Angerhausen, L. Dorogin, H. Murrenhoff and B. N. J. Persson (2018). Influence of anisotropic surface roughness on lubricated rubber friction: Extended theory and an application to hydraulic seals. Wear, 410, 43–62.

[20] M. M. Reddi, "Finite-element solution of the incompressible lubrication problem." (1969): 524–533.

[21] M. Scherrer, R. Scheidl, E. Luckachev. A new elastic non contacting sealing concept for valves. 2020 IEEE Global Fluid Power Society PhD Symposium, October 19–21, 2020, online.

[22] D. Bartel, 'Verallgemeinerte Reynolds'sche Differenzialgleichung', in Simulation von Tribosystemen: Grundlagen und Anwendungen, D. Bartel, Ed. Wiesbaden: Vieweg+Teubner, 2010, pp. 21–37. doi: 10.1007/978-3-8348-9656-8_2.

[23] G. Tatsumi, M. Ratoi, Y. Shitara, S. Hasegawa, K. Sakamoto, B. G. Mellor, Mechanism of oil-lubrication of PEEK and its composites with steel counterparts, Wear, Volumes 486–487, 2021, 204085.

[24] W. Wieleba, T. Lesniewski, D. Elemes, A. Elemes, Friction Process of selected Polymers sliding on steel and duralumin in a lubricant envirnoment, Tribologia 4-2016.
[25] N. Patir, H. S. Cheng, An average flow model for determining effects of threedimensional roughness on partial hydrodynamic lubrication, Journal of Lubrication Technology, Vol. 100, 1978.
[26] R. Rituraj, R. Scheidl, Stability Analysis of Spools with Imperfect Sealing Gap Geometries, International Journal of Fluid Power, Vol. 21 3, 383–404.

Biographies

Matthias Scherrer was awarded his master's degree in mechatronics from the Johannes Kepler University (JKU) Linz, Austria, in 2018. He is currently studying for his PhD at the Institute of Machine Design and Hydraulic Drives at the JKU and his research centres on simulations and the experimental study of hydraulic components and systems, especially exoskeleton actuations. He also has experience of working in industry in the field of hydraulics for Hainzl Industriesysteme.

Rudolf Scheidl completed both his M.Sc. in mechanical engineering and PhD in engineering sciences at the Vienna University of Technology. He has experience in the research and development of agricultural machinery (Epple Buxbaum Werke), continuous casting technology (Voest-Alpine Industrieanlagenbau) and paper mills (Voith). Since 1990, he has been a full Professor of mechanical engineering at the Johannes Kepler University, Austria. His research focuses on hydraulic drive technology and mechatronic design.